

Generalized confocal imaging systems for free-space optical interconnections

Qing Cao, Matthias Gruber, and Jürgen Jahns

A generalized confocal imaging system, which is composed of two confocal lenses and one field lens, is proposed for free-space optical interconnections. Unlike in a conventional $4-f$ system, both the object distance and the image distance can be almost arbitrarily chosen. This advantage is especially important for practical setups in which the object distance and the image distance cannot be designed to be the same. As a concrete example, we have designed and experimentally tested a planar-integrated micro-optical imaging system. The result is in good agreement with the theoretical prediction. Similarly to the conventional $4-f$ imaging system and the light-pipe imaging system, the system proposed here can also be used as one important part of a hybrid imaging setup. © 2004 Optical Society of America

OCIS codes: 200.4650, 350.3950, 110.1650, 050.1940, 080.2730.

1. Generalized Confocal Imaging System

The conventional $4-f$ system is widely used for imaging in free-space optical interconnections because it offers telecentricity and good imaging performance for extended fields. It is also an important part of a hybrid $4-f$ imaging system.^{1,2} As shown in Fig. 1, one characteristic feature of this setup is that object distance d_1 , image distance d_2 , and focal length f are the same. However, design restrictions in practical setups, for example, for planar-integrated free-space optical interconnections,^{3,4} often do not allow one to choose the parameters d_1 , d_2 , and f in this way. To overcome this disadvantage and to provide additional design freedom, we propose here a generalized confocal imaging system, shown in Fig. 2, for free-space optical interconnections.

It is well known that propagation through paraxial optical systems can be described by matrix optics.^{5,6} In matrix optics, a specific transfer is denoted by a specific $ABCD$ matrix, which has the form

$$\begin{bmatrix} A & B \\ C & D \end{bmatrix},$$

The authors are with Optische Nachrichtentechnik, FernUniversität Hagen, Universitätsstrasse 27/PRG, 58084 Hagen, Germany. Q. Cao's e-mail address is qing.cao@fernuni-hagen.de.

Received 3 November 2003; revised manuscript received 9 March 2004; accepted 22 March 2004.

0003-6935/04/163306-04\$15.00/0

© 2004 Optical Society of America

where A – D are the four matrix elements. According to matrix optics,^{5,6} total transfer matrix M from the input plane to the output plane in Fig. 2 can easily be determined to be

$$\begin{aligned} M &= \begin{bmatrix} 1 & d_2 \\ 0 & 1 \end{bmatrix} \begin{bmatrix} 1 & 0 \\ -f^{-1} & 1 \end{bmatrix} \begin{bmatrix} 1 & f \\ 0 & 1 \end{bmatrix} \begin{bmatrix} 1 & 0 \\ -F^{-1} & 1 \end{bmatrix} \begin{bmatrix} 1 & f \\ 0 & 1 \end{bmatrix} \\ &\times \begin{bmatrix} 1 & 0 \\ -f^{-1} & 1 \end{bmatrix} \begin{bmatrix} 1 & d_1 \\ 0 & 1 \end{bmatrix} \\ &= \begin{bmatrix} -1 & 2f - d_1 - d_2 - \frac{f^2}{F} \\ 0 & -1 \end{bmatrix}. \end{aligned} \quad (1)$$

It is well known that the intensity distribution at the output plane is the image of that at the input plane when matrix B is equal to 0. Then, from Eq. (1), one can get the following imaging condition for the setup of Fig. 2:

$$d_1 + d_2 + f^2/F = 2f. \quad (2)$$

Also according to matrix optics,^{5,6} when the imaging condition $B = 0$ is satisfied, the value of matrix element A indicates the magnification. From Eq. (1) one can see that the magnification is -1 , where the negative sign indicates a coordinate reversal. We find that the conventional $4-f$ setup corresponds to the special case of $F = \infty$ and $d_1 = d_2 = f$. We also find that the light-pipe imaging system^{7–9} corresponds to another special case of $d_1 = d_2 = 0$ and $F = f/2$. Because the two f lenses still have a common focal plane and added field lens F is located just at

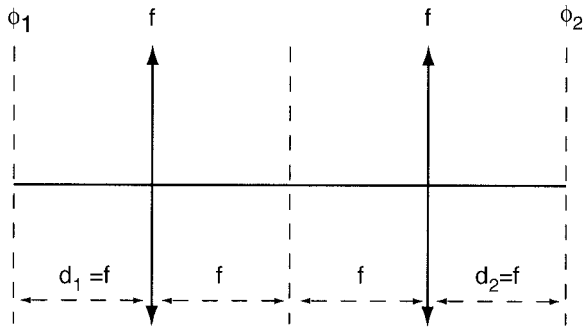


Fig. 1. Schematic view of the conventional 4- f system.

this plane, we call this imaging system a generalized confocal imaging system. For predetermined f , d_1 , and d_2 values, one can always find a suitable F value to make the equality of Eq. (2) hold. This advantage significantly improves design freedom and flexibility. The solution for F can be given explicitly by

$$F = f^2 / (2f - d_1 - d_2). \quad (3)$$

When $2f > d_1 + d_2$, the field lens is a positive lens because $F > 0$. When $2f < d_1 + d_2$, the field lens is a negative lens because $F < 0$. When $2f = d_1 + d_2$, the field lens is not needed because $F = \infty$. It is worth mentioning that the relaxed design freedom still has limits that are imposed by the lens technology used. Limitations exist, for example, for the range of focal lengths that can be implemented, the numerical aperture, and the efficiencies.¹⁰

2. Experimental Test As an Example

As one concrete application of the generalized confocal imaging system mentioned above, we designed and experimentally tested a planar-integrated micro-optical imaging system. As shown in Fig. 3, this folded system images the input signal at the input plane into the corresponding position at the output plane, through a zigzag path. We denote by x and z the transverse and the vertical directions, respectively, of the cross plane shown in Fig. 3. The y direction is that which is perpendicular to the cross plane. We denote by OS the optical substrate used in this test system. We denote by IP, OP, G, f , F , and M the input plane, the output plane, a grating that

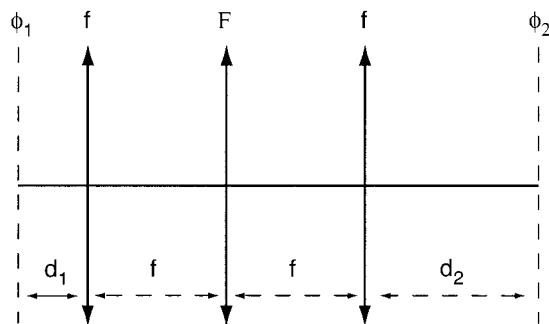


Fig. 2. Schematic view of the generalized confocal imaging system.

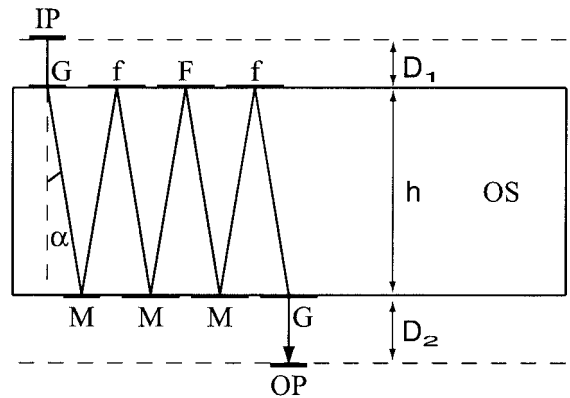


Fig. 3. Schematic view of a planar-integrated micro-optical imaging system.

deflects the light, a confocal lens, the field lens, and a reflective mirror, respectively. The reflective mirrors are made from highly reflective metal films. The lenses are reflective multilevel diffractive lenses with four phase levels. They are designed in accordance with their relationship to elliptical Fresnel zone plate lenses after the related focal lengths have been determined. They are fabricated by means of two-mask binary photolithography and reactive-ion etching upon the optical substrate. For efficiency, highly reflective metal films deposited upon surfaces to cover the diffractive lenses. For each diffractive lens, the x -directional size is 1.8 mm and the y -directional size is 4.55 mm. A photo of the central part of an f lens is shown in Fig. 4. For the layout of Fig. 3 the input plane might, for example, consist of an array of vertical-cavity surface-emitting laser sources or modulators bonded onto the substrate directly or onto an intermediate substrate, such that distance D_1 to the substrate will be short. In our experiment, thickness h of the optical substrate, distance D_1 between the input plane and the top plane of the substrate, distance D_2 between the output plane and the bottom surface of the substrate, and deflection angle α are chosen such that $h = 9$ mm, $D_1 = 1$

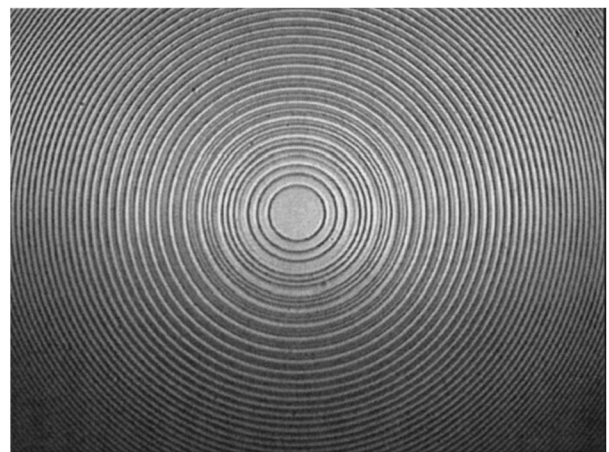


Fig. 4. Photo of the central part of an f lens.

mm, $D_2 = 0.688$ mm, and $\alpha = 5.711^\circ$. The optical substrate is chosen to be fused silica, whose refractive index is $n = 1.453$ at the vacuum wavelength $\lambda = 850$ nm. Simply by using the value of the refractive index and of relation $\Lambda = \lambda/[n \sin(\alpha)]$, we determine both periods Λ of the input grating and the output grating to be $5.879 \mu\text{m}$. According to the structure of Fig. 3, focal length f of the confocal lenses, object distance d_1 , and image distance d_2 are determined to be $f = 18$ mm, $d_1 = 2f + nD_1 = 19.453$ mm, and $d_2 = f + nD_2 = 10$ mm, respectively. By the way, we use $d_1 = 2f + nD_1$ and $d_2 = f + nD_2$ rather than $d_1 = 2f + D_1$ and $d_2 = f + D_2$ because the fused silica substrate has refractive index 1.453, which is different from refractive index 1 of free space. The lengths D_1 and D_2 in free space are equivalent to the lengths nD_1 and nD_2 in the fused-silica substrates, respectively. Substituting the values of f , d_1 , and d_2 into Eq. (3), one can get $F = 49.488$ mm. In the above calculations of f , F , d_1 , and d_2 , we did not take into account the oblique propagation property of the light. That is to say, we still assume that the planar-integrated optical system is a normal paraxial optical system in which all the components have a common optical axis; strictly speaking, such is not the case. However, the differences and the connections between a planar-integrated optical system and its corresponding unfolded optical system are investigated in detail in Refs. 11 and 12. It is shown that^{11,12} the lenses in a planar-integrated optical system are not circular lenses but elliptical lenses. That is to say, the x - and the y -directional focal lengths are slightly different. According to the analyses of Refs. 11 and 12, the x - and the y -directional focal lengths of the f lens and the F lens are determined to be $f_x = f/\cos^3(\alpha) = 18.271$ mm, $f_y = f/\cos(\alpha) = 18.090$ mm, $F_x = F/\cos^3(\alpha) = 50.233$ mm, and $F_y = F/\cos(\alpha) = 49.735$ mm, respectively. It is worth mentioning that, for each of these lenses, the difference between the x and the y directions is small, because the difference between the x - and the y -directional focal lengths is small. One can easily verify this fact by taking a look at Fig. 4.

We fabricated and experimentally tested this planar-integrated micro-optical imaging system. As shown at the left in Fig. 5, we employed a 4- f system to relay the light source of a laser diode with a wavelength of 850 nm into a suitable position at an input plane that is ~ 1 mm (i.e., distance D_1 in Fig. 3) in front of the left-hand surface (i.e., the top surface in Fig. 3) of the planar optical system. This relayed light source was used as the input object. The focal lengths of the two relay lenses are both 40 mm. There are two principal reasons for the use of the relayed light source rather than the direct light source. One is to prevent damage of the elements that may result from contact during the adjustment because the distance from the object to the left-hand surface of the optical substrate is very short (only 1 mm). The other is that the holder of the optical substrate used in the experiment does not permit a short distance only, between the direct light source

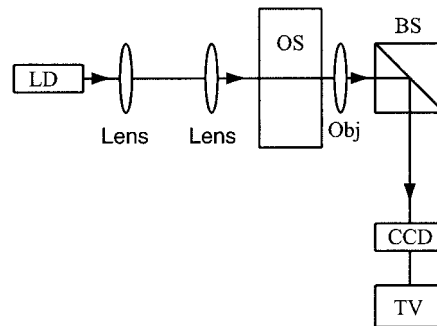


Fig. 5. Experimental arrangement for testing the planar-integrated micro-optical imaging system. We denote by LD, OS, Obj, and BS the laser diode, the optical substrate, the micro-objective, and the beam splitter, respectively.

and the left-hand surface of the planar-optical-system. As shown at the right of Fig. 5, we used a large-working-distance micro-objective to image a suitable plane onto the CCD receiver plane with suitable magnification (this is actually a microscope) and used a TV for observation. By using this large-working-distance micro-objective we can observe not only the right-hand surface (and its neighborhood) but also the left-hand surface (and its neighborhood) of the planar optical system by adjusting the position of the micro-objective. The experimental result is in good agreement with the design. By adjusting the position of the micro-objective we could clearly observe both the input object of the laser spot at the input plane and the corresponding output image at the output plane. Photos of the input object and the corresponding output image are shown in Fig. 6. We may not be sure that there is no distortion, but we are sure that the potential distortion is small. For practical applications, the receiving targets normally have sizes of dozens of micrometers by dozens of micrometers. From Fig. 6 one can see that these sizes are much larger than the spot size of the image. Therefore, for practical applications, the potential small distortion can be ignored. As we stated above, there is a coordinate reversal between the object and

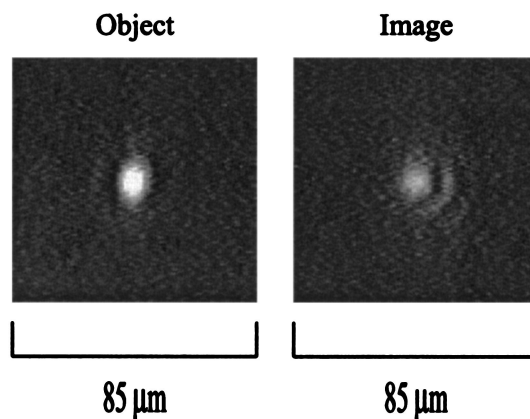


Fig. 6. Photos of the input object and the corresponding output image.

the image. This property cannot easily be shown by the image itself of a pointlike object. However, this coordinate reversal can be easily shown by the locations of the pointlike object and of the corresponding pointlike image. For example, if the pointlike object shifts a certain distance in the positive (or the negative) y direction, then the pointlike image will shift a certain distance but in the opposite direction. We did indeed observe this kind of behavior in the experiment, which accordingly demonstrated the property of coordinate reversal. In summary, the experiment has directly demonstrated the good performance of the generalized confocal imaging system.

3. Conclusions

Based on matrix optics,^{5,6} we have proposed a generalized confocal imaging system for free-space optical interconnections. This imaging system is composed of two confocal lenses and a field lens. Both the conventional $4f$ imaging system and the light-pipe imaging system⁷⁻⁹ are special cases of this generalized confocal imaging system. By adjusting focal length F of the field lens, one can almost arbitrarily choose object distance d_1 and image distance d_2 . This advantage significantly improves design freedom and flexibility. At the same time, this generalized imaging system still keeps the advantage of telecentricity of the conventional $4f$ system. As a concrete application, we designed and experimentally tested a planar-integrated micro-optical imaging system. The result is in good agreement with the theoretical prediction. Similarly to the conventional $4f$ imaging system and the light-pipe imaging system,⁷⁻⁹ this proposed system can also be used as one important part of the hybrid imaging setup.^{1,2}

The authors thank their colleagues for support and discussions. This study was financially supported by the Deutsche Forschungsgemeinschaft. The authors are indebted to the reviewers for their comments and suggestions for improving the paper.

References

1. A. W. Lohmann, "Image formation of dilute arrays for optical information processing," *Opt. Commun.* **86**, 365-370 (1991).
2. J. Jahns and B. Acklin, "Integrated planar optical imaging system with high interconnection density," *Opt. Lett.* **18**, 1594-1596 (1993).
3. J. Jahns and A. Huang, "Planar integration of free-space optical components," *Appl. Opt.* **28**, 1602-1605 (1989).
4. J. Jahns, "Planar packaging of free-space optical interconnections," *Proc. IEEE* **82**, 1623-1631 (1994).
5. N. Hodgson and H. Weber, *Optical Resonators* (Springer-Verlag, Berlin, 1997), Chaps. 1 and 2.
6. J. W. Goodman, *Introduction to Fourier Optics*, 2nd ed. (McGraw-Hill, New York, 1996), pp. 401-413.
7. S. Sinzinger and J. Jahns, "Integrated micro-optical imaging system with a high interconnection capacity fabricated in planar optics," *Appl. Opt.* **36**, 4729-4735 (1997).
8. K.-H. Brenner, W. Eckert, and C. Passon, "Demonstration of an optical pipeline adder and design concepts for its microintegration," *Opt. Laser Technol.* **26**, 229-237 (1994).
9. N. Streibl, R. Völkel, J. Schwider, P. Habel, and N. Lindlein, "Parallel optoelectronic interconnections with high packing density through a light-guiding plate using grating couplers and field lenses," *Opt. Commun.* **99**, 167-171 (1993).
10. S. Sinzinger and J. Jahns, *Microoptics*, 2nd ed. (Wiley, Weinheim, Germany, 2003), Subsec. 6.3.6 and Sec. 2.1.
11. M. Testorf and J. Jahns, "Paraxial theory of planar integrated systems," *J. Opt. Soc. Am. A* **14**, 1569-1575 (1997).
12. M. Testorf and J. Jahns, "Imaging properties of planar-integrated micro-optics," *J. Opt. Soc. Am. A* **16**, 1175-1183 (1999).